

1
2
3
4
5
6
7
8
9
10
11
12
13
14
15
16
17
18
19
20
21

Using Fractal Analysis of Crown Images to Measure the Structural Condition of Trees

**Jon Murray^{1*}, George Alan Blackburn¹, James Duncan Whyatt¹
and Christopher Edwards²**

¹ Lancaster Environment Centre, Lancaster University, Lancaster, LA1 4YQ

*² School of Computing and Communications, Lancaster University, Lancaster,
LA1 4WA.*

*Corresponding author: Tel: +44 1524 652 01; Email: j.murray3@lancaster.ac.uk

Observations of tree canopy structure are routinely used as an indicator of tree condition for the purposes of monitoring tree health, assessing habitat characteristics or evaluating the potential risk of tree failure. Trees are assigned to broad categories of structural condition using largely subjective methods based upon ground-based, visual observations by a surveyor. Such approaches can suffer from a lack of consistency between surveyors; are qualitative in nature and have low precision. In this study, a technique is developed for acquiring, processing and analysing hemispherical images of sessile oak (*Quercus petraea* (Matt.) Liebl.) tree crowns. We demonstrate that by calculating the fractal dimensions of tree crown images it is possible to define a continuous measurement scale of structural condition and to be able to quantify intra-category variance of tree crown structure. This

22 approach corresponds with traditional categorical methods; however, we recognise that further
23 work is required to precisely define interspecies thresholds. Our study demonstrates that this
24 approach has the potential to form the basis of a new, transferable and objective methodology that
25 can support a wide range of uses in arboriculture, ecology and forest science.

26 **Introduction**

27 Traditionally the assessment of tree structural condition, as used in general tree surveys, relies upon
28 simple methodologies and ground-based observations due to the physical complexities of directly
29 measuring tree crowns. However, these traditional techniques are time consuming, manual and
30 largely subjective. Subjectivity has been shown to prevent the same conclusions being reached
31 during independent tree surveys, including surveys of the same trees by different, experienced tree
32 surveyors (Norris 2007). Predominantly these assessments rely on a tree surveyor's knowledge of
33 ideal tree form, tree health, their ability to identify pests and disease, and the consideration of
34 potential hazards and targets that are at risk of harm. Blennow, Persson et al. (2013) state that when
35 managing trees or woodlands the use of subjective tree condition observations are not ideal,
36 particularly where objective tree assessments would provide greater insights in the tree
37 management decision process. Ultimately, traditional tree assessment procedures can result in
38 subjective and potentially biased, field observations of tree condition, irrespective of how
39 knowledgeable and experienced the surveyor is (Norris 2007, Britt and Johnston 2008).

40 Trees are self-optimising organisms that respond to a range of recurrent environmental demands
41 and employ strategies to alter their form to minimise potential negative effects or optimise their
42 structure for the greatest physiological benefit (Zimmerman and Brown 1971, Mattheck and Breloer
43 1994, Fourcaud, Dupuy et al. 2004, Pollardy 2008). In most angiosperms, the lateral branches grow
44 almost as fast, or in some instances faster, than the terminal leader. This process results in the
45 characteristic broad crown structure common in this tree type (Pollardy 2008, Burkhart and Tome
46 2012). Tree form is typically the result of various influences combining the genetic potential, the

47 demands of physiological processes, spatial competition in the crown and the effects of other
48 environmental conditions, such as thigmomorphogenic change caused by repeated wind force
49 effects. The shedding of branches through responsive self-pruning driven by abscission, is a
50 characteristic found in many tree species which has a direct effect on the shape of the crown
51 (Pollardy 2008).

52 There are many additional reasons for trees to shed branches, or parts thereof; which are
53 accelerated by the effects of colonising pathogens e.g. fungal infestation, or external forces such as
54 gravity or wind force. Indeed, the tree's own physiology also increases the potential for crown
55 dieback as trees age (King 2011). Despite many potential stimuli affecting overall tree structure, the
56 growth habits of trees are fundamentally controlled by the genetic predisposition of individual
57 species throughout different tree growth stages. Therefore, the characteristic structure and form of
58 differing tree species remain visually recognisable even after the external impacts are considered
59 (Zimmerman and Brown 1971). When trees reach late-maturity, there is a combined slowing down
60 of both the stem diameter increment and extension growth in the crown, as a response of the
61 influence of the tree species, genotype or its local environment (King 2011). It is the recognition of
62 these types of biotic and abiotic structural changes that tree surveyors use to aid the classifying of
63 trees into discrete categories, ultimately aiming to gain insights into the tree's condition.

64 There have been many studies of tree crown structure in recent years, many of which utilise high-
65 end technology such as light detecting and ranging (LiDAR) as the main method of data capture
66 (Ørka, Næsset et al. 2009, Ferraz, Saatchi et al. 2016). Specifically with LiDAR data investigations, it is
67 understood that the success of tree investigation algorithms for location detection or height
68 estimation is strongly correlated to the type of tree structure under analysis (Vauhkonen, Ene et al.
69 2012). Through analysis of aerial LiDAR data, boreal tree species have been identified at a species
70 level due to differences in their tree structure signatures (Lina and Hyyppä 2016), or through LiDAR
71 waveform analysis which identifies structural features within the LiDAR wave (Hovi, Korhonen et al.

72 2016). Aerial LiDAR investigations are often supported with aerial imagery which is captured
73 simultaneously as image based investigations also provide opportunities for tree canopy structure
74 analysis (Dash, Watt et al. 2016). Furthermore, photogrammetric techniques such as digital stereo
75 imagery and radar imagery have been used in tree canopy structure investigations (Holopainen,
76 Vastaranta et al. 2014). For many researchers or environmental managers, a restrictive element of
77 these types of investigations is the requirement for expensive, specialised research equipment that
78 is often mounted on an aerial platform, such as an unmanned aerial vehicle (UAV), aeroplane or
79 satellite.

80 The use of hemispherical photography to undertake proximal tree crown assessments has a field
81 history of more than 50 years, with forest ecologists, Evans and Coombe (1959) using the technique
82 to investigate the available light climate under woodland canopies with an early prototype 'Hill' (fish
83 eye) camera. This has remained a readily used, accessible and repeatable method for the
84 investigation of tree canopy structure (Hale 2004, Chianucci 2016). Researchers have also previously
85 used hemispherical imagery to assess canopy gap fraction or provide leaf area index assessments
86 (Weiss, Baret et al. 2004, Beckschäfer, Seidel et al. 2013), as it is understood that images captured by
87 hemispherical, or fisheye, lenses provide opportunities for photogrammetric measurement
88 (Schwalbe, Maas et al. 2009). Conducting photogrammetric analysis on hemispherical imagery falls
89 within the remote, or indirect, methods of measurement which enable rapid, non-destructive
90 determination of crown properties (Chason, Baldocchi et al. 1991, Weiss, Baret et al. 2004). Modern
91 advancements in digital cameras, coupled with readily available hemispherical lenses or lens
92 adapters, provide the opportunity for an off-the-shelf approach to photogrammetric research
93 (Leblanc, Chen et al. 2005).

94 When tree crowns are viewed from directly beneath, looking upwards towards the zenith viewing
95 point (90° from the horizontal elevation), holes can be observed within the crown structure. The
96 tree crown area is a complex arrangement of tree branches, combined with observable unoccupied

97 areas between the different parts of the tree crown. This upward looking view provides a visual
98 separation between the tree structure and the sky, which when photographed can be converted into
99 a binary image with the occupied and background regions of the image coded '1' and '0' respectively
100 (Beckschäfer, Seidel et al. 2013, Sossa-Azuela, Santiago-Montero et al. 2013). Image analysis
101 techniques for pattern recognition in tree structures have identified features of lacunarity (the size
102 and distribution of holes), complex spatial distributions or other morphologic features (Zheng, Gong
103 et al. 1995, Frazer, Wulder et al. 2005).

104 Due to the unique geometry found in nature, the dimensions of natural, physical forms cannot
105 readily be described in simple, integral terms (Mandelbrot 1982, Dimri 2000). Mandelbrot (1982)
106 argues that more insightful measurements are required to measure pattern complexity, such as
107 quantifying the degree of complexity in a structure. As trees exhibit natural structural variance,
108 Mandelbrot (1982), also notes that it is the frequently anomalous nature of tree structure whose
109 form is sculpted by, "chance, irregularities and non-uniformity", that provides the opportunity for
110 statistical investigation. Rian and Sassone (2014) demonstrate that the crown structures of trees are
111 unique in their self-affine and highly irregular branching patterns. It has been stated that fractal
112 dimensions (D_f) can be used to quantify structural complexity in a continuous measure, theoretically
113 ranging from 0 to infinity, which can be expressed as a single value (Mandelbrot 1967, Kaye 2008).
114 Although tree crown structures are complex shapes, there are various examples of D_f being used as
115 a predictor variable for the classification of forest canopies (Zeide and Pfeifer 1991, Zeide 1998,
116 Jonckheere, Nackaerts et al. 2006, Zhang, Samal et al. 2007).

117 The aim of this study was to develop an objective methodology to assess the structural condition of
118 broadleaved tree crowns (*Quercus sp.*) by quantifying the complexity of the tree crowns through
119 hemispherical images taken under leaf-off conditions. This approach was designed to overcome the
120 limitations of current subjective field methodologies. The first objective was to develop an in-field
121 data capture technique that was suitable for a range of subject trees across a variety of structural

122 conditions. The second objective was to develop image processing methods for the assessment of
123 crown structural condition. The third objective was to propose a new and objective means of
124 evaluating tree structural condition on a continuous scale.

125 **Methodology**

126 Throughout three study areas across northwest Lancashire, England, 64 Sessile Oak trees (*Quercus*
127 *petraea* (Matt.) Liebl.) were individually photographed using hemispherical imagery obtained from
128 beneath subject tree canopies, looking towards the zenith viewpoint (Figure 1). The trees used in the
129 study were either individual maiden trees, or trees that were located in closed canopy, woodland
130 conditions. The trees were photographed over a single winter season in leaf-off condition, thereby
131 allowing an unobscured view of the tree crown structure. To minimise potentially confounding
132 variables, this method was applied to trees of the same species that were in the mature phases of
133 tree development, specifically: early-mature (28%), mature (25%), late-mature (25%), veteran and
134 senescent (22%) (Fay and de Berker 1997). To achieve a suitable sample size, a locally prolific species
135 was used in this study.

136 **Figure 1 near here**

137 **Field Methodology Development**

138 Reference data on the trees structural condition was collected using a four-point categorical system,
139 as is common in arboricultural assessments using traditional field techniques. The four-point method
140 used in this research is not based upon a single specific method, but broadly upon several
141 arboricultural tree survey methods (e.g. BS5837:2012 surveys which use a four level condition
142 hierarchy, the ISA tree hazard evaluation, which uses four classification categories to generate an
143 accumulative hazard score (Matheny and Clark 1994, BSI 2012), and is also comparable with a
144 qualitative tree condition category assignment as described in Swetnam, O'Connor et al. (2016)).
145 Consequently, this approach is representative of similar tree survey methods where the assessment

146 of trees leads to an empirical categorisation of tree condition. Box 1 provides an overview of the
147 classification descriptors.

148 **Box 1 near here**

149 Once identified, the tree's cardinal orientation was determined by the use of a field compass. The
150 part of the crown that extended towards the southernmost point (i.e. the tree crown's southern
151 axis), was marked out along the ground with a standard surveyors tape and used as the linear axis
152 upon which the crown images were taken at specific intervals.

153 **Camera Set-up**

154 A high-resolution digital single-lens reflex (dSLR) camera (Canon EOS 550D DS126271) was used with
155 an 18mm lens and a hemispherical lens adapter (Opteka Super Wide Fisheye Lens 0.20X). The lens
156 adapter permits focal length conversion into a 3.6mm circular lens. The wide angle of the
157 hemispherical lens enabled as much of each tree crown to be captured within each image as
158 possible. The dSLR was placed on a standard photographic tripod, adjusted at each image capture
159 location ensuring that the dSLR was positioned and levelled with the camera lens pointing vertically
160 upward at ~0.5m from the ground level. To account for variability in solar illumination, the images
161 were taken during uniform sky conditions. These conditions occur predominantly when the sky is
162 overcast, although this technique can also be used just before sunrise or just after sunset, should
163 bright daytime conditions be expected (Song, Doley et al. 2014).

164 **Image Acquisition and Spatial Sampling Strategy**

165 Initially, the number of images captured per subject tree was influenced by the overall length of the
166 crown along the southern axis. Early trials with image capture involved taking images at 1m intervals
167 along the southern axis, to the full extent of the crown. However, this produced a high number of
168 replicates with large amounts of image content overlap. Inspection of these images identified two

169 problems with this approach. Firstly, that there was ~90% replication of content between the
170 overlapping images (Figure 2a), and secondly, that additional tree features that were not required
171 for the analysis were also captured. For example, additional stem wood was photographed in the
172 images closest to the base of the tree (e.g. at 1m and 2m intervals), while large amounts of 'sky' was
173 captured towards the canopy edge. Neither of these image components was required in the analysis.
174 It followed that many of the repeated images was not within the optimal range for representing the
175 fullest area of tree crown within an image. Repeated testing indicated that the optimal location for
176 image capture was around the mid-point of the crown axis (Figure 2). Where there was no mid-point
177 location on an exact 1m interval of the southern axis mid-point, the distance was rounded up to the
178 next whole metre. The southern axis was used for standardisation purposes as the subject trees are
179 located in the Northern hemisphere and our preference was to capture images on the non-shaded,
180 south facing side of the trees.

181 **Figure 2 near here**

182 Immediately after acquisition, the quality of each image was visually assessed. This step was taken to
183 ensure the images were suitable for later analysis and to allow additional images to be captured
184 should the original image be unusable. The process of identifying the southern axis, setting-up the
185 camera and completing image acquisition took between ~45 seconds to ~1.5 minutes, depending on
186 the complexity of the local topographic environment.

187 **Image Preparation**

188 Upon return from the field, the images were re-examined on a desktop computer to check for image
189 clarity, suitability in showing the area of interest, and for the presence of key features (Jones and
190 Vaughn 2010). A limitation of the in-field image proofing was that this was completed on the dSLR
191 camera's 2.7-inch screen; therefore it was conducted at a very coarse resolution. Of the original 247
192 images, 87 were removed for blurring or distortion errors, 96 images were removed as duplicates,

193 leaving the sample size reduced to 64 images of individual trees, with a single image representing
194 each tree.

195 Pre-processing interventions removed errors from the images that could affect the measurement of
196 image metrics. Chromatic aberration (CA) is the misregistration of RGB channels causing interference
197 with the dSLR Bayer-pattern sensor, leading to image deterioration and interference with pixel-
198 based classification techniques (Schwalbe, Maas et al. 2009). In this study, CA was corrected by
199 removing the red and blue channels, and converting the image to the green element of the RGB
200 channels only. Quadratic or 'barrel' distortion is also associated with images captured using
201 hemispherical lenses. A distortion correction algorithm (Vries 2012) transformed the images from
202 the distorted barrel extension to replicate an image captured at a normal focal length. This
203 perspective distortion effect is influenced by the relative distances between the lens and subject
204 canopy at which the image is captured, therefore, it is important that the relative distance was
205 maintained during image capture. In order to reduce the effects of blurred images caused by
206 contrast errors between colour ranges, an image sharpening algorithm was used. This algorithm was
207 based upon un-sharp masking, where the image is sharpened by removing a blurred negative copy
208 of the same image. The copied mask was laid over the original, resulting in a combined image that is
209 visually sharper. Where there were instances of unsuccessful pre-processing, the affected images
210 were not used in the investigation.

211 The images were analysed in Matlab (2015a), where each image pixel was indexed and converted
212 into binary form. This was achieved through applying uniform quantization where limited intensity
213 resolution breaks the image colour space into individual pixels, which are indexed, and the pixel
214 locations are mapped. A process of dithering corrects any potential quantization errors and limits
215 the greyscale range of the image. This binarization procedure allows differentiation between the
216 tree structure and other parts of the image, as optimum image analysis conditions are best achieved
217 where there is high contrast between tree structure and the sky (Chen, Black et al. 1991).

218 **Defining the Image Analysis Area**

219 Chianucci and Cutini (2012), describe that it is beneficial in image processing to reduce the field of
220 view by masking some elements of the full hemisphere, thereby achieving greater spatial
221 representation of heterogeneous tree crowns i.e. the inclusion of both dense and sparse crown
222 regions in the analysis. At Figure 2b, image analysis is restricted to the part of tree canopy contained
223 within the black bounding box, created on a per image basis. The analysis extent is influenced by
224 standard forestry measurement conventions (West 2009), with the lower bounding box edge
225 originating at the point of estimated timber height. In decurrent trees, this is where the main stem
226 bifurcates to such a degree that the main stem is no longer discernible. From here, the analysis area
227 is bordered by the upper bounding box at the edge of the tree crown and avoids the image's
228 vignette region caused by the visible inner walls of the camera lens. The left and right boundaries of
229 the image analysis area are demarked by adjoining lines between the upper and lower bounding box
230 extents maximising the crown analysis area, while again, also avoiding the vignette region at the
231 edges of the image.

232 **Predictor Variable Creation**

233 Multiple indices were generated from the tree images that were developed into image metrics
234 which were tested, both individually and in combination, for their suitability in describing the tree
235 structural character. A description of the metrics is shown at Table 1.

236 **Table 1 near here**

237 Euler numbers represent the amount of tree crown occupied by solid tree structure through
238 quantifying connected pixel components, holes and vertices within the image. Initially an RGB image
239 is indexed and an inverse colour map algorithm restricts the number of possible RGB colour values
240 to a predetermined range, e.g. 32, 48 or 64 colours, to refine the image resolution. Each pixel is then
241 matched to the closest colour in the colour map, and the image is subsequently binarised for

242 analysis purposes. Euler numbers are then used to measure image topology through the frequency
243 and area occupancy of 'holes' within the binarised image. These holes are subtracted from the total
244 number of objects that occupy the image region, therefore the Euler value represents pixel
245 occupation in the image (Chen and Yan 1988). The creation of the Euler number is defined as:

$$E = N - H \tag{1}$$

246 where N is the number of connected image components (region), and H is the number of image
247 holes identified as separate from the region (Sossa-Azuela, Santiago-Montero et al. 2013).

248 Convex hulls are used to delineate a computed shape edge; therefore in this application, region
249 convex hulls are considered representative of the tree crown edge extent and provide the
250 opportunity to quantify the area covered by the hull shape. Region convex hulls were created
251 demarking a polyhedron boundary in the Euclidean plane around a known distribution of data points
252 (X). This process defines a measurable boundary where the polygon is considered convex if all of the
253 dataset X lie within the boundary, and any two points in X can be joined using a straight-line
254 segment that also remains within the boundary. A limitation of convex hulls is that the outer bounds
255 of the polygon may extend beyond the data range in order to maintain convexity, thereby
256 potentially adding additional area to the generated polygon. Successful convex hull algorithms
257 however, provide the smallest convex contour area within a given region (Gargano, Bellotti et al.
258 2007).

259 A similar method used in photogrammetric analysis is the calculation of equivalent diameters. The
260 projections of equivalent diameters are frequently used in RS investigations to model the spatial
261 distribution of tree crowns. Within this study the equivalent diameter metric represents the area
262 occupied by the tree crown structure in each image, while also providing a potentially continuous
263 index of equivalent circle areas. A scalar value is defined that is the equivalent area of the irregular
264 shape within the image (Kara, Sayinci et al. 2013), and is compared to the area of a known shape,
265 e.g. a circle, using the equation;

$$d_e = \sqrt{(4a/\pi)} \quad (2)$$

266 where a is the area of the irregular shape, and d_e is the equivalent diameter.

267 Finally, in order to quantify the complexity of the tree crown structure, a fractal geometric analysis
 268 approach was used to assess each image for self-affinity by calculating the logarithmic mean for the
 269 Df of each image. Df is used as a measure of complexity as Mandelbrot (1967) recognised the merits
 270 of using Df to quantify complex change in pattern detail relative to scale. Fractal dimensions should
 271 be considered an approximation of the Kolmogorov capacity, driven by a recursive process where
 272 small elements of the image are analysed individually, before the overall Kolmogorov capacity for
 273 the image is calculated. Equation 3 describes the Df calculation:

$$Df = \lim_{R \rightarrow \infty} \ln N(R)/\ln(R) \quad (3)$$

274 Where N is the number of boxes needed to cover the fractal shape where it is present, R represents
 275 the unit size of the boxes, and $N(R)$ is the number of boxes required to fulfil the fractal element for
 276 the image region. *Lim* refers to the limit of R , as R approaches infinity (Bonnet, Bour et al. 2001,
 277 Moisy 2008). In order to generate an individual Df model, a box-counting function (Moisy 2008) is
 278 applied that derives a local Df at each box size, integrated with the power law:

$$N(R) = N_0 * R^{-Df} \quad (4)$$

279 where N_0 is the expected value when R equals one. As this approach is dependent on both R and Df
 280 the result is a logarithmic mean of all the Df values generated for the fractal region of the image, and
 281 is interpreted as a quantification of the structural complexity of tree crowns. The steps required to
 282 process the tree images and compute individual tree metrics are summarised at Figure 3Figure 3.

283 **Calculating Statistical Probabilities**

284 The suitability of the predictor variables in quantifying tree structure was tested via multinomial
 285 regression, where the observed tree conditions are categorical responses, given as:

$$\log\left(\frac{\pi_i^{(j)}}{\pi_i^{(0)}}\right) = \alpha^{(j)} + \beta_1^{(j)}X_{1i} + \dots + \beta_k^{(j)}X_{ki} \quad (5)$$

286 where X_{ki} is the k^{th} predictor variable for i , the imaginary unit. 0 is the reference standard, j is the
 287 non-reference standard, and $\alpha^{(j)}$ and $\beta_1^{(j)}, \dots, \beta_k^{(j)}$ are the various unknown population parameters.
 288 The predictor variables are used to discern where a response, i.e. the tree structure, relates to the
 289 same tree characteristics that are indicative of an observed condition. Multinomial regression
 290 therefore, creates a proportional odds model where a single category of trees is specified as the
 291 reference standard and is used as a comparative measure against which all other tree categories are
 292 compared. Probability (P) estimates are calculated for all trees, to quantify the likelihood that they
 293 share the same structural characteristics as the reference standard trees. For the purposes of this
 294 study, 'Good' category trees (Box 1), are used as the reference standard. The probability that the
 295 non-reference standard trees share the same structural characteristics of the reference standard is
 296 expressed as a P estimate percentage.

297 **Outlining Classification Thresholds**

298 To allow the comparison of continuous and categorical data, several predictor variables were used
 299 to create quantified indices to represent the structural character of the individual trees (Table 1).
 300 These variables were analysed to discriminate between the structural characteristics of individual
 301 trees and to determine how well the indices represented the field-observed classification. The
 302 predictor variable indices were grouped and analysed as individual indices, i.e. all Df values grouped
 303 as one data set, all Euler (64) values as another data set etc.

304 An empirical data mapping test was undertaken where homogeneity traits were observed in the
 305 predictor variable indices. Data mapping is achieved where the categorical data is plotted over the
 306 ordinal data using the two available values for each tree image e.g. categorical: Good,
 307 ordinal/predictor value: Df 1.875. The tree images were grouped by their field-observed

308 classifications; Good, Moderate, Poor and Dead. For each of these four groups, the minimum and
309 maximum predictor indices values showed the threshold value extent for each classification.

310 **Results**

311 At Figure 4a, the Df predictor variable quantifies the structural characteristics of all the assessed
312 trees with individual Df values on a continuous scale, and displays homogenous clustering of the
313 field-observed condition types. The group threshold extents are demarked as horizontal
314 classification lines for the Df predictor variable in Figure 4a, where there are four separate groups of
315 Df values consistent with their given field classifications; Good, Moderate, Poor and Dead (Table 2).
316 In instances where heterogeneity was observed in the predictor variable indices, the data mapping
317 could not be applied and it was not possible to define threshold extents (Figure 4b-d).

318 **Table 2 near here**

319 At Figure 4b-d, there are heterogeneous clusters of field classifications as denoted by the mixed
320 colouring and absence of threshold lines. All sub-plots in Figure 4 show similarities with generally
321 decreasing indices, suggesting a continuous nature to the data, and implying that the trees included
322 in the study possessed a varying range of structural conditions. In Figure 4b, c and d, all field-
323 observed conditions are shown in heterogeneous grouping for the different predictor variable
324 indices, therefore demonstrating inconsistency with the field-observed classification for each
325 predictor variable (Table 1). It follows that the remaining predictor variables (Table 1 and Figure 4 b-
326 d) do not provide a suitable mechanism to discriminate between different structural characteristics.

327 **Figure 3 near here**

328 Euler (64) (Figure 4b.) is the only variable to output negatively skewed data, and repeatedly
329 quantified a number of individual trees with a Euler value of '1', thereby also providing limited
330 information on potential structural differences in these trees. Figure 4a shows the validity of Df as a
331 continuous measure of tree structure complexity. We further demonstrate the relationship between

332 the categorical classifications and the probability that Df values are representative of these
333 categories in Figure 5. Within the good category, there is a ~99% probability that the trees share the
334 same structural characteristics as the trees in the reference standard. Within the moderate category,
335 the probability that the trees show the same structural characteristics of a good tree structure has
336 fallen to ~89% at the median, thereby identifying a probability shift between good and moderate
337 structural characteristics. There is a further, large median shift between the moderate and poor
338 categories, as the median reduces to ~29% for poor category trees when compared to the reference
339 standard. Where trees were field-observed as belonging in the dead category, there is a decrease in
340 probability to <1% that these trees show the same structural characteristics as the reference
341 standard.

342 **Figure 5 near here**

343 Also in Figure 5, it is noticeable that there is no overlap between the overall visible spread (OVS) in
344 the good field-observed population and any of the other potential categories, due to the OVS
345 separation between all other field-observed categories. Similarly, this trend of OVS separation
346 continues for each field-observed category when compared to any other category. Trees quantified
347 as having structural characteristics of either the moderate or poor groups have a larger interquartile
348 range than trees observed to be in either good or dead condition. This indicates that there is a
349 greater degree of uncertainty in characterising the moderate or poor groups of trees, particularly as
350 the trees with the good or dead characteristics, are assigned to their relative categories with a high
351 degree of precision. In order to identify potential subgrouping effects, where similar classification
352 probabilities may be clustered around specific probability values, a linear regression model was
353 calculated which identified that there was no evidence of subgrouping and that the probability data
354 range is randomly spread ($r^2 = 0.86$, P -value 0.01).

355 **Discussion**

356 This study presents a methodology for the objective assessment of tree crown structure, through
357 analysing tree crown structure in hemispherical images. The underlying aim of this study is to reduce
358 the degree of subjectivity currently accepted within tree surveying and assessment, and to provide
359 opportunities for high resolution intra-category assessment of tree structure. Mandelbrot (1967)
360 states that the question of how to accurately measure tree crowns, with the inherent complexity of
361 objectively assessing various shapes, forms, structural porosity, all of varying sizes, is not a simple
362 task that can be solved with classical geometry. Following the findings of this study, it is possible to
363 quantify tree structural complexity using Df as an objective predictor variable using a relatively
364 proximal photogrammetric method and computational analysis (Figure 4), thereby increasing the
365 objectivity and repeatability of structural assessment, whilst also reducing the potential for bias from
366 field measurements.

367 Through quantifying tree structure in Df and creating a proportional odds model, the probabilities
368 that field-observed, 'good' classified trees displayed the structural characteristics of structurally
369 sound trees, was found to be statistically very high at $P \sim 99\%$. Due to the way the proportional odds
370 model functions, achieving this high level of probability is essential for the reliable characterisation
371 of the remaining structural condition types. It is suggested that this method of analysis could be
372 transferred to many other investigations of tree structure where the model is trained on a species-
373 specific basis across differing structural architectures.

374 Following the creation of the model, the probabilities of trees with moderate, poor or dead
375 observed classes reduce at the median to $P \sim 89\%$, $P \sim 29\%$ and $P < 1\%$ respectively when compared to
376 the reference standard images (Figure 5). These changes in median levels reflect a measured
377 reduction of the tree crown structure complexity. The continuous nature of the Df scale provides a
378 unique measurement of individual tree structure characteristics, as opposed to individual trees
379 being arbitrarily grouped into coarse-resolution, homogenous categories where intra-category
380 differences cannot be easily identified. This insight provides the researcher or practitioner with the

381 opportunity to further sub-divide each classification group, and to monitor intra-category variance
382 over time. This methodology has the potential for the long-term monitoring of pest, disease or
383 pathogen progression, or for the quantification of structural decline, particularly with trees of high
384 conservation, landscape or heritage value. This could include the monitoring of naturally occurring
385 veteran trees, to quantify their rate of structural decline, particularly in areas where there is
386 potential conflict with the public. Furthermore, this method could also be used to guide and inform
387 the process of tree veteranisation, where pre-veteran, mature trees are intentionally injured and
388 receive structural alterations to mimic the structure of naturally occurring veterans with the aim of
389 providing valuable habitats that would otherwise only be found on the most mature trees
390 (Bengtsson, Hedin et al. 2012).

391 As shown in Figure 4a there is a wide range of Df values, homogenous grouping of field-
392 observations, and no clustering of the *P* ranges for each potential category. Therefore, it can be
393 stated that tree structure is more accurately quantified in a structural condition continuum than
394 with traditional categorical classification methods. Tree structure measurably degenerates the more
395 trees senesce; tree crown structures change as branch death and limb shedding occur, which
396 ultimately leads to a general decrease in the fractal nature of tree crowns (Mäkelä and Valentine
397 2006). Through understanding phenotypic tree structures and the biological response of trees to
398 environmental stress, there is the potential to relate tree structure complexity to an overall
399 indication of tree health or general condition. Tree crown structures are indicative of the amount of
400 photosynthetically active area in the tree required for homeostatic equilibrium, and therefore is
401 considered to act as a reliable indicator of tree health (Burkhart and Tome 2012).

402 An advantage of this method is the potential to measure intra-category differences in tree structure
403 complexity and with the computerised storage and easy retrieval of this data, the same analysis can
404 be repeated over time, allowing the accurate tracking of tree structure change. Sudden catastrophic
405 damage to a tree crown is readily recognisable, such as when following a strong wind event.

406 However, more subtle or prolonged tree crown degeneration as a result of biotic or abiotic stress;
407 such as pathogen ingress, or sudden death as a result of heavy, late frosts, could be measured and
408 identified over repeat iterations of surveying. It is recognised that in the immediate period after the
409 sudden death of a tree via these more subtle means, that the structure will likely not have changed
410 significantly, and although potentially dead, a tree could still be classified as good due to the
411 immediate retention of its 'good' structure, further reinforcing the requirement for temporal studies
412 to monitor the subtle changes of the tree crown. Further developments of this method should
413 include a refinement of the methodology to accurately measure more subtle structural change in the
414 finer structures of the crown edge.

415 The traditional coarse categorical classification methods do not provide a clear mechanism for
416 measuring subtle structural degeneration as the thresholds for the each potential category are
417 poorly defined and only provide generalised categories for the tree classification. For tree-risk
418 managers such as local government tree officers or utility company infrastructure managers, a
419 structural condition continuum can be used to objectively quantify the probabilities that their tree
420 stock is in a suitable condition. Through quantifying tree structure in a continuous Df scale, specific,
421 measurable thresholds for remedial intervention may be defined. With a categorical approach, tree-
422 risk managers have the limitation of allocating broad categories such as 'poor' or 'dead' as the
423 triggers for remedial intervention. This limitation greatly increases the number of trees that will be
424 designated as requiring remedial work, compounded by the additional costs and labour
425 requirements. As a higher resolution method, our new approach has the potential to limit
426 unnecessary remedial works, lowering tree management expenditure, and would facilitate limited
427 resources being used in more focussed interventions. We acknowledge that additional work is
428 required to quantify the extent of these improvements, particularly in respect to health and safety
429 related tree management

430 This investigation used a single broadleaved tree species, and we recognise that further work is
431 required to determine where categorical thresholds exist for other tree species. This would follow
432 the work of Morse, Lawton et al. (1985), who observed that there are differences in the structural
433 complexity of varying vegetation species when they are measured in Df. During a pilot study phase,
434 we identified that there are different thresholds for condition categories in different tree species.
435 The other broadleaved species photographed in various quantities prior to this investigation, were;
436 *Acer pseudoplatanus* (L.), (*Fraxinus excelsior* (L.), *Quercus rubra* (L.), *Fagus sylvatica* (L.), *Betula*
437 *pubescens* (Ehrh.), *Crataegus monogyna* (Jacq.), and *Pinus sylvestris* (L.). Initial observations suggest
438 that there are likely to be interspecies differences from the small sample numbers used, therefore,
439 this research could also be extended to consider other tree species.

440 In training the reference category for the proportional odds model, trees that are observed as being
441 in a sound structural condition and are representative of trees in good condition for that species, are
442 identified as the reference category trees. These become the standard against which the remaining
443 trees of the same species are compared. In the process of developing the model, a small degree of
444 user intervention is required to define the parameters of the model and to interpret the model
445 efficacy. Similarly, a user defined bounding box is created to identify the area of interest for the
446 image analysis. This method ensures the procedure can be applied across the full range of tree
447 crown images. The creation of the bounding box is governed by the user following a set of standards
448 that are influenced by standard forestry conventions (West 2009), and the simple requirement to
449 only identify the tree crown of interest and no other elements, such as the image vignette region. An
450 important distinction to highlight is that the procedure remains a dependable and independent
451 methodology, despite the user intervention as the image analysis, statistical querying and
452 computation of the Df value are all autonomous and therefore, remain objective. This methodology
453 does not purport to entirely remove the requirement for practitioner intervention. We also
454 recognise a potential limitation of this methodology is the reliance on the southern axis for capturing
455 crown images. During methodology development, the southern axis was used to standardise

456 fieldwork when capturing tree crown images. It is recommended that additional field trials should be
457 undertaken to determine the sensitivity of capturing images from differing cardinal points or
458 multiple locations per tree.

459 **Conclusion**

460 The methodology described in this study for assessing the structural condition of trees is
461 commensurate with traditional techniques. The development of a proximal, hemispherical image
462 field methodology enabled the data capture of many trees in a range of different physical conditions
463 and locations, and satisfies the first objective of this study. The second objective was met with the
464 analysis and objective measurement of hemispherical tree structure images. Finally the ranking of
465 individual trees by the automated calculation of the continuous Df values, satisfies the third
466 objective. It can be stated that the traditional techniques which identify broad categories of
467 structural condition are very coarse, as they do not account for intra-category structural variability
468 and are highly subjective. Our approach enables the assessment of tree condition to be completed
469 with a greater level of precision than was previously possible due to the continuous nature of the Df
470 measurement. Fundamentally, this concept provides a repeatable and objective way to characterise
471 tree crown structure, which can be used to improve the objectivity of tree surveying and inform the
472 specific management of trees with high amenity value. We recognise that further work is required to
473 define the sensitivity of the image acquisition protocol, and to gain further understanding of the full
474 extent of intra-species differences. Nonetheless, it is envisaged that this methodology could form
475 the basis for a new range of analytical measures that will enable tree, environmental or ecological
476 managers to gain greater insights and make more informed decisions about the tree stock under
477 their management.

478 **Funding**

479 This research is supported by an Engineering and Physical Sciences Research Council (EPSRC)
480 studentship for the lead author [EP/L504804/1].

481 **Supplementary Information**

482 The following supplementary material is available at *Forestry* online: Statistical analysis of the image
483 pre-processing effect on the predictor variable, Df, and a recommended workflow for field
484 operations, data collection and processing.

485 **Acknowledgements**

486 The lead author would like to thank Dr. V. Karloukovski, Lancaster Environment Centre, Lancaster
487 University, for discussions on fractal dimensions, and, Dr. E. Eastoe, Department of Mathematics and
488 Statistics, Lancaster University, for providing statistical advice. The authors would also like to thank
489 the anonymous reviewers for their valuable comments and suggestions to improve the quality of
490 this paper.

491 **Conflict of interest statement**

492 None declared.

493

494

References

495

496 Barrell, J. (1993). "Pre-planning Tree Surveys: Safe Useful Life Expectancy (SULE) is the Natural
497 Progression." Arboricultural Journal **17**(1): 33-46.

498 Barrell, J. (2001). SULE: Its Use and Status into the New Millennium. NAAA Arboricultural
499 Conference. Sydney, Australia, NAAA

500 Beckschäfer, P., D. Seidel, C. Kleinn and J. Xu (2013). "On the Exposure of Hemispherical Photographs
501 in Forests." iForest – Biogeosciences and Forestry **6**: 228-237.

502 Bengtsson, V., J. Hedin and M. Niklasson (2012). Veteranisation of Oak – Managing Trees to Speed
503 Up Habitat Production. Trees Beyond the Wood. Sheffield, International Union of Forest Research
504 Organisations (IUFRO): 1-11.

505 Blennow, K., J. Persson, A. Wallin, N. Vareman and E. Persson (2013). "Understanding Risk in Forest
506 Ecosystem Services: Implications for Effective Risk Management, Communication and Planning."
507 Forestry **87**(2): 219-228.

508 Bonnet, E., O. Bour, N. E. Odling, P. Davy, I. Main, P. Cowie and B. Berkowitz (2001). "Scaling of
509 Fracture Systems in Geological Media." Reviews of Geophysics **39**(3): 347–383.

510 Britt, C. and M. Johnston (2008). Trees in Towns II. London, Department for Communities and Local
511 Government.

512 BSI (2012). Trees in Relation to Design, Demolition and Construction - Recommendations. B. S.
513 Institute, BSI Standards Limited.

514 Burkhart, H. E. and M. Tome (2012). Modelling Forest Trees and Stands. New York, Springer.

515 Chason, J. W., D. D. Baldocchi and M. A. Huston (1991). "A Comparison of Direct and Indirect
516 Methods for Estimating Forest Canopy Leaf Area " Agricultural and Forest Meteorology **57**: 107-128.

517 Chen, J. M., T. A. Black and R. S. Adams (1991). "Evaluation of Hemispherical Photography for
518 Determining Plant Area Index and Geometry of a Forest Stand." Agricultural and Forest Meteorology
519 **56**(1-2): 129-143.

520 Chen, M.-H. and P.-F. Yan (1988). "A Fast Algorithm to Calculate the Euler Number for Binary
521 Images." Pattern Recognition Letters **8**(5): 295-297.

522 Chianucci, F. (2016). "A Note on Estimating Canopy Cover from Digital Cover and Hemispherical
523 Photography." Silva Fennica **50**(1): 1-10.

524 Chianucci, F. and A. Cutini (2012). "Digital Hemispherical Photography for Estimating Forest Canopy
525 Properties: Current Controversies and Opportunities." iForest **5** 290-295.

526 Dash, J. P., M. S. Watt, S. Bhandari and P. Watt (2016). "Characterising Forest Structure Using
527 Combinations of Airborne Laser Scanning Data, RapidEye Satellite Imagery and Environmental
528 Variables." Forestry **89**: 159 –169.

529 Dimri, V. P. (2000). Application of Fractals in Earth Sciences. Rotterdam, Netherlands., A.A. Balkema.

- 530 Evans, G. C. and D. E. Coombe (1959). "Hemispherical and Woodland Canopy Photography and the
531 Light Climate." Journal of Ecology **47**(1): 103-113.
- 532 Fay, N. and N. de Berker (1997). Veteran Trees Initiative Specialist Survey Method. Peterborough,
533 UK., English Nature.
- 534 Ferraz, A., S. Saatchi, C. Mallet and V. Meyer (2016). "Lidar detection of individual tree size in tropical
535 forests." Remote Sensing of Environment **183**: 318-333.
- 536 Fourcaud, T., L. Dupuy, D. Sellier, P. Ancelin and P. Lac (2004). Analysis of the Relationship Between
537 Tree Structure and Biomechanical Functions. 4th International Workshop on Functional-Structural
538 Plant Models (FSPM04), Montpellier, France.
- 539 Frazer, G. W., M. A. Wulder and K. O. Niemann (2005). "Simulation and Quantification of the Fine-
540 scale Spatial Pattern and Heterogeneity of Forest Canopy Structure: A Lacunarity-based Method
541 Designed for Analysis of Continuous Canopy Heights." Forest Ecology and Management **214**: 65-90.
- 542 Gargano, G., R. Bellotti, F. de Carlo, S. Tangaro, E. Tommasi, M. Castellano, P. Cerello, S. C. Cheran
543 and C. Fulcheri (2007). A novel Active Contour Model algorithm for contour detection in complex
544 objects. 2007 IEEE International Conference on Computational Intelligence for Measurement
545 Systems and Applications.
- 546 Hale, S. (2004). Managing Light to Enable Natural Regeneration in British Conifer Forests. F.
547 Commission. Edinburgh, Forestry Commission: 1-6.
- 548 Holopainen, M., M. Vastaranta and J. Hyypä (2014). "Outlook for the Next Generation's Precision
549 Forestry in Finland." Forests **5**(7): 1682-1694.
- 550 Hovi, A., L. Korhonen, J. Vauhkonen and I. Korpela (2016). "LiDAR waveform features for tree species
551 classification and their sensitivity to tree- and acquisition related parameters." Remote Sensing of
552 Environment **173**: 224-237.
- 553 Jonckheere, I., K. Nackaerts, B. Muys, J. V. Aardt and P. Coppin (2006). "A Fractal Dimension-based
554 Modelling Approach for Studying the Effect of Leaf Distribution on LAI Retrieval in Forest Canopies "
555 Ecological Modelling **197**: 179-195.
- 556 Jones, H. G. and R. A. Vaughn (2010). Remote Sensing of Vegetation: Principles, Techniques and
557 Applications. Oxford, Oxford University Press.
- 558 Kara, M., B. Sayinci, E. Elkoca, I. Öztürk and T. B. Özmen (2013). "Seed Size and Shape Analysis of
559 Registered Common Bean (*Phaseolus vulgaris* L.) Cultivars in Turkey Using Digital Photography."
560 Journal of Agricultural Sciences **19**: 219-234.
- 561 Kaye, B. H. (2008). A Random Walk Through Fractal Dimensions. West Sussex, England., John Wiley
562 and Sons.
- 563 King, D. A. (2011). Size Related Changes in Tree Proportions and Their Potential Influence on the
564 Course of Height Growth. Size and Age Related Changes in Tree Structure and Function. F. C.
565 Meinzer, B. Lachenbruch and T. E. Dawson. New York, Springer Science. **4**.
- 566 Leblanc, S. G., J. M. Chen, R. Fernandes, D. W. Deering and A. Conley (2005). "Methodology
567 Comparison for Canopy Structure Parameters Extraction from Digital Hemispherical Photography in
568 Boreal Forests." Agricultural and Forest Meteorology **129**: 187-207.

569 Lina, Y. and J. Hyypä (2016). "A Comprehensive but Efficient Framework of Proposing and
570 Validating Feature Parameters from Airborne LiDAR Data for Tree Species Classification."
571 International Journal of Applied Earth Observation and
572 Geoinformation **46**: 45-55.

573 Lonsdale, D. (1999). The Principles of Tree Hazard Assessment and Management. London, HMSO.

574 Mandelbrot, B. (1967). "How Long Is the Coast of Britain? Statistical Self-Similarity and Fractional
575 Dimension." Science **156**(3775): 636-638.

576 Mandelbrot, B. (1982). The Fractal Geometry of Nature. San Francisco, W. H. Freeman and Company.

577 Matheny, N. P. and J. R. Clark (1994). A Photographic Guide to the Evaluation of Hazard Trees in
578 Urban Areas, International Society of Arboriculture.

579 Mattheck, C. and H. Breloer (1994). The Body Language of Trees: A Handbook for Failure Analysis.
580 London, The Stationary Office.

581 Md Rian, I. and M. Sassone (2014). "Tree-inspired dendriforms and fractal-like branching structures
582 in architecture: A brief historical overview." Frontiers of Architectural Research **3**(3): 298-323.

583 Moisy, F. (2008). boxcount. Paris, Université Paris Sud.

584 Morse, D. R., J. H. Lawton, M. M. Dodson and M. H. Williamson (1985). "Fractal Dimension of
585 Vegetation and the Distribution of Arthropod Body Lengths." Nature **314**: 731-733.

586 Mäkelä, A. and H. T. Valentine (2006). "Crown Ratio Influences Allometric Scaling in Trees." Ecology
587 **87**(12): 2967–2972.

588 Norris, M. (2007). Tree Risk Assessments – What Works – What Does Not –Can We Tell?
589 International Society of Arboriculture; Australia Chapter (ISAAC) Conference, Perth, Australia.,
590 International Society of Arboriculture; Australia Chapter.

591 NTSG (2011). Common Sense Risk Management of Trees. Guidance on Trees and Public Safety in the
592 UK for Owners, Managers and Advisers. Edinburgh, Forestry Commission.

593 Pollardy, S. G. (2008). Physiology of Woody Plants. USA, Elsevier.

594 Schwalbe, E., H.-G. Maas, M. Kenter and S. Wagner (2009). "Hemispheric Image Modelling and
595 Analysis Techniques for Solar Radiation Determination in Forest Ecosystems." Photogrammetric
596 Engineering & Remote Sensing **75**(4): 375–384.

597 Song, G.-Z., D. Doley, D. Yates, K.-J. Chao and C.-F. Hsieh (2014). "Improving Accuracy of Canopy
598 Hemispherical Photography by a Constant Threshold Value Derived from an Unobscured Overcast
599 Sky. ." **44**: 17-27.

600 Sossa-Azuela, J. H., R. Santiago-Montero, M. Pérez-Cisneros and E. Rubio-Espino (2013). "Computing
601 the Euler Number of a Binary Image Based on a Vertex Codification." Journal of Applied Research
602 and Technology **11**(3): 360-370.

603 Swetnam, T. L., C. D. O'Connor and A. M. Lynch (2016). "Tree Morphologic Plasticity Explains
604 Deviation from Metabolic Scaling Theory in Semi-Arid Conifer Forests, Southwestern USA." PLoS ONE
605 **11**(7): e0157582.

606 Vauhkonen, J., L. Ene, S. Gupta, J. Heinzl, J. Holmgren, J. Pitkänen, S. Solberg, Y. Wang, H.
607 Weinacker, K. M. Hauglin, V. Lien, P. Packalén, T. Gobakken, B. Koch, E. Næsset, T. Tokola and M.
608 Maltamo (2012). "Comparative testing of single-tree detection algorithms under different types of
609 forest." Forestry: An International Journal of Forest Research **85**(1): 27-40.

610 Vries, J. d. (2012). Barrel and Pincushion Lens Distortion Correction, Mathworks.

611 Weiss, M., F. Baret, G. J. Smith, I. Jonckheere and P. Coppin (2004). "Review of methods for in situ
612 leaf area index (LAI) determination: Part II. Estimation of LAI, errors and sampling." Agricultural and
613 Forest Meteorology **121**(1-2): 37-53.

614 Weiss, M., F. Baret, G. J. Smith, I. Jonckheere and P. Coppin (2004). "Review of Methods for In-situ
615 Leaf Area Index (LAI) Determination Part II. Estimation of LAI, Errors and Sampling." Agricultural and
616 Forest Meteorology **121**: 37-53.

617 West, P. W. (2009). Tree and Forest Measurement. London, Springer Science & Business Media.

618 Zeide, B. (1998). "Fractal analysis of foliage distribution in loblolly pine crowns." Canadian Journal of
619 Forest Research **28**(1): 106-114.

620 Zeide, B. and P. Pfeifer (1991). "A Method for Estimation of Fractal Dimension of Tree Crowns."
621 Forest Science **37**(5): 1253-1265.

622 Zhang, D., A. Samal and J. R. Brandle (2007). "A Method for Estimating Fractal Dimension of Tree
623 Crowns from Digital Images." International Journal of Pattern Recognition and Artificial Intelligence
624 **21**(3): 561-572.

625 Zheng, X., P. Gong and M. Strome (1995). "Characterizing Spatial Structure of Tree Canopy Using
626 Colour Photographs and Mathematical Morphology." **21**(4).

627 Zimmerman, M. H. and C. L. Brown (1971). Trees: Structure and Function. New York, Springer-Verlag.

628 Ørka, H. O., E. Næsset and O. M. Bollandsås (2009). "Classifying species of individual trees by
629 intensity and structure features derived from airborne laser scanner data." Remote Sensing of
630 Environment **113**(6): 1163-1174.

631

632

633

634

635

636 **Tables**

Table 1 Descriptions of analytical metrics used in an investigation to quantify tree structural condition.

Name	Description
Convex Hull Area	An area value of the smallest potential convex polygon used to envelop the indexed region in a p-by-2 matrix.
Equivalent Diameter	A scalar value for a computed circle with the same area as the indexed image.
Euler Number (32)	A scalar value that specifies the frequency of indexed objects in the image region. The Euler number subtracts porosity values (holes) representative of crown porosity using 32-bit imagery.
Euler Number (48)	A scalar value that specifies the frequency of indexed objects in the image region. The Euler number subtracts porosity values (holes) representative of crown porosity using 48-bit imagery.
Euler Number (64)	A scalar value that specifies the frequency of indexed objects in the image region. The Euler number subtracts porosity values (holes) representative of crown porosity using 64-bit imagery.
Filled Area	A scalar count identifying the number of pixels used to ‘fill-in’ the indexed image (removal of image/crown porosity), with the count extending to the full perimeter of the structure using a logical test of the region index.
Fractal Dimension	A continuous, scaled measurement of self-affinity, where repeating x and y curves are magnified by different factors and a logarithmic mean is calculated.

637

638

639 Table 2 Threshold limits of tree condition categories, expressed in fractal dimensions (Df).

Field Categories	Df Threshold
Good	≥ 1.6021
Moderate	≤ 1.6020 to > 1.4815
Poor	≤ 1.4814 to > 1.3423
Dead	≤ 1.3422

640

641

642

643 **Box Caption**

Box 1 Classification descriptors for the subjective arboricultural assessment of trees. Estimated Remaining Contribution (ERC) refers to a methodology used to consider the health, condition and structure of the tree and aids in classifying the tree in to the different categories *adapted from* (Barrell 1993, Lonsdale 1999, Barrell 2001, NTSG 2011, BSI 2012). Note: The images show trees in leaf-on condition to enable ease of comparison for the condition types.

644 **Illustrations Captions**

Figure 1 A schematic of the field method for taking a hemispherical picture from beneath a tree canopy. The camera is situated on a standard tripod, and is levelled and pointing towards the zenith viewing point (90° from the horizontal elevation). In this example, the full extent of the crown is four metres along the southern axis, and the image is taken at the two metre mid-point.

645

Figure 2 A schematic showing the optimised range for image capture (a), and the area of tree canopy structure analysed within this study (b). The area of interest is specifically the structural elements of the canopy. Too much 'sky' within the image reduces the amount of structure that can be analysed (a). Stem wood and other elements not required, are removed from the image by only analysing the structure inside a user selected bounding box area (b). The use of a bounding box allows images of both individual trees and trees within closed canopies to be analysed.

646

Figure 3 A procedural workflow showing how tree structure images are processed for the computation of image metrics.

647

Figure 4 Sample subset of predictor variables used to define the characteristics of different tree structures (*n*64). The annotations Good, Moderate, Poor and Dead refer to the field observed condition of the individual trees. Only with the measure of fractal dimension (a.), provides homogeneous clustering of field observed conditions as identified by the threshold lines. Not all predictor variables used in this study are visualised in this plot.

648

Figure 5 A proportional odds model to indicate the probability (*P*) that tree structure images, quantified in fractal dimensions (Df), are indicative of an observable tree structure condition and known reference standard (*n*64). Tree images were measured for structural complexity in Df. The box plot extents identify the *P* that the structures show characteristics of the reference standard.

4. Good

Dominant trees. Full crown, good extension growth and form. Typical for age and species. High number of buds. Healthy reaction growth to any injuries. Acceptable levels of colonisation. ERC: >40+ years



3. Moderate

Some signs of stress, crown dieback or retrenchment. Deadwood. Other signs of stress likely to be present. Remedial work may have previously taken place. Cavities rot or early disease may be present. ERC: ≥10-40 years



2. Poor

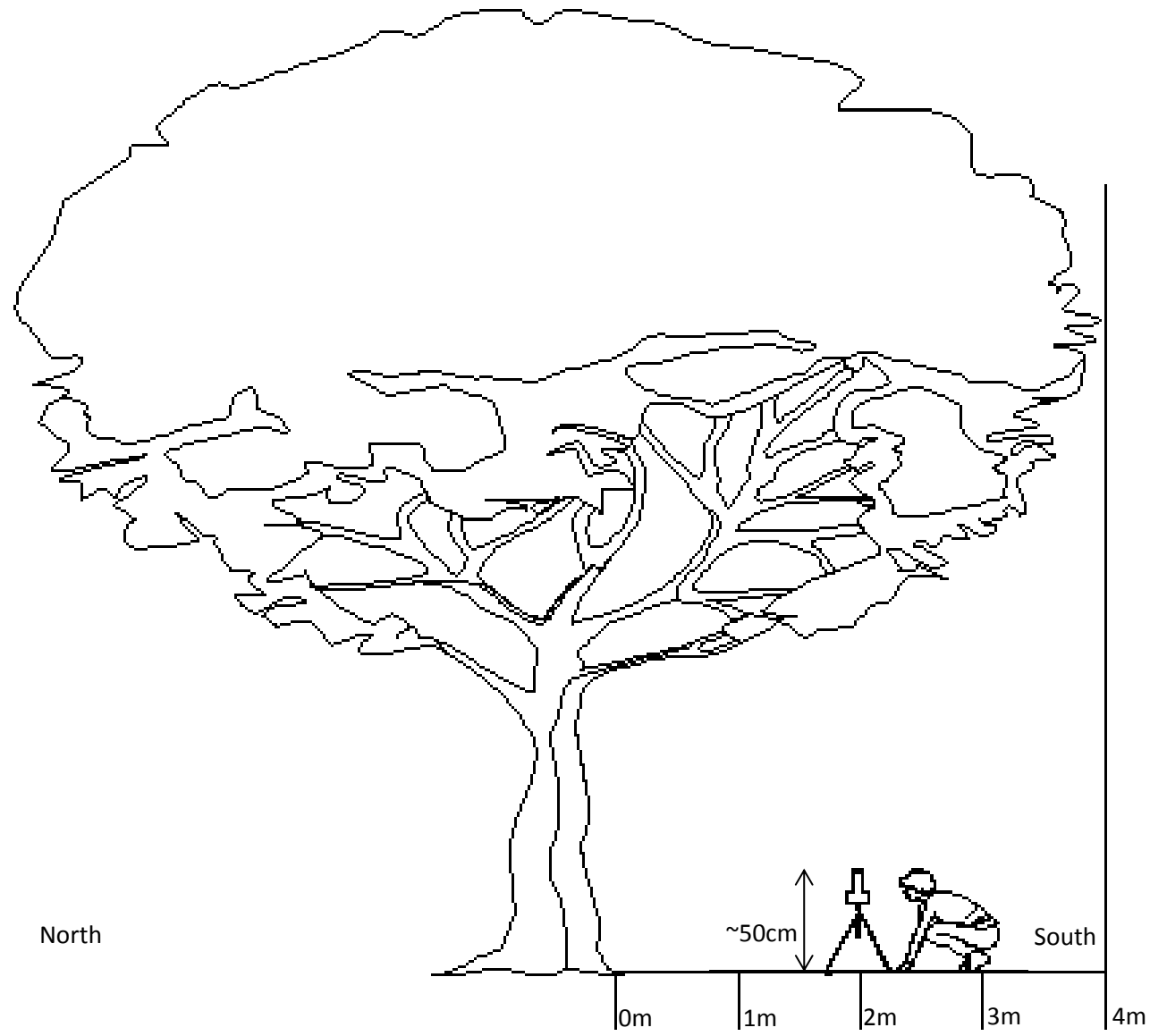
Obvious signs of dieback. Frequent deadwood. Clear signs of disease and decay. Overwhelming of the trees natural defences. Colonisation by fungi, wood boring insects and other decay biota highly likely. ERC: ≤10 years



1. Dead

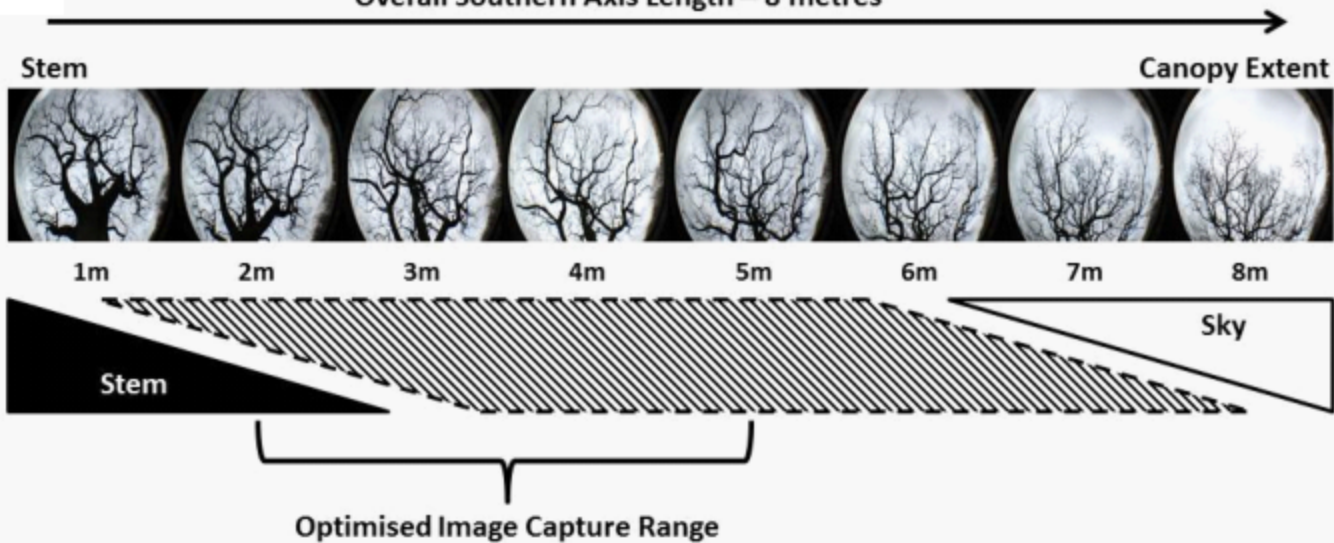
Physiological processes have ceased. Lack of active photosynthetic area. Colonisation of fungi, wood boring insects and other decay biota highly likely. Extensive crown retrenchment, bark slough, brittle or collapsing structure. ERC: ≤ 0 years



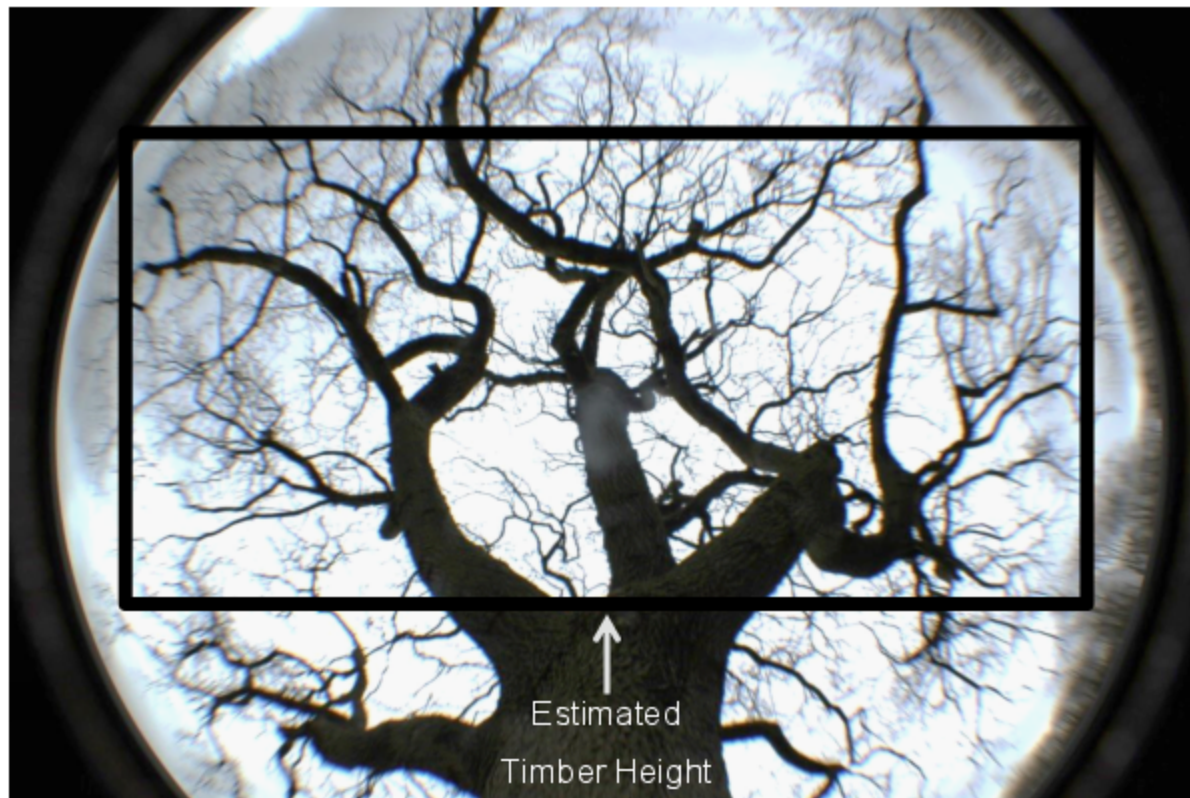


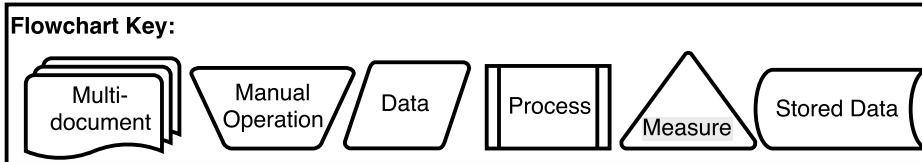
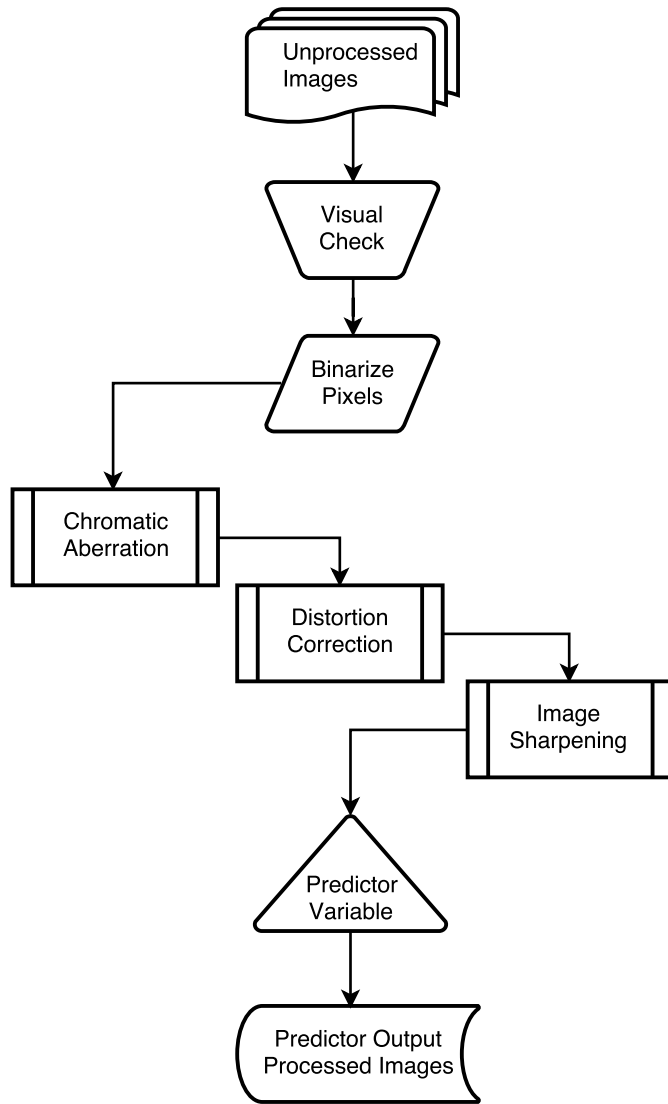
a.

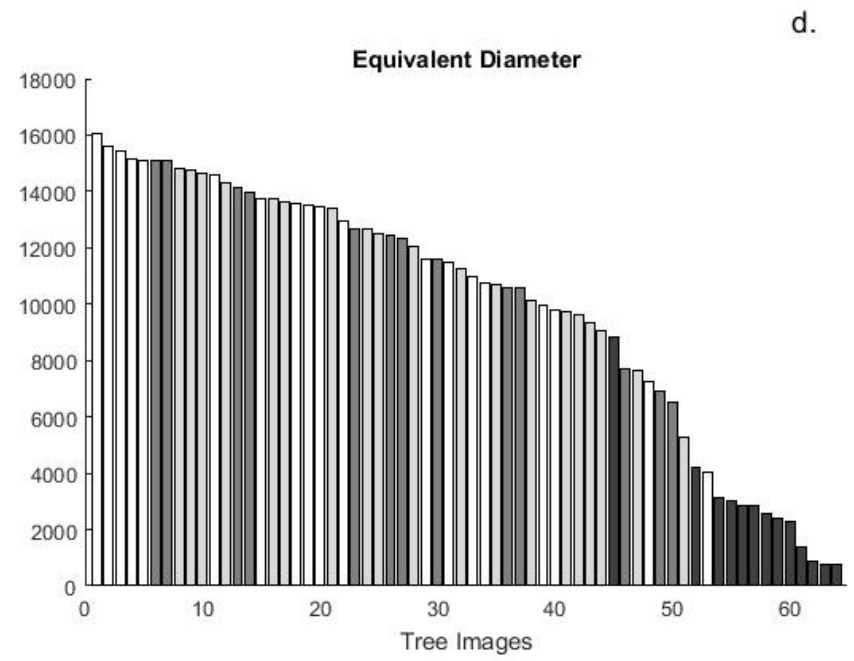
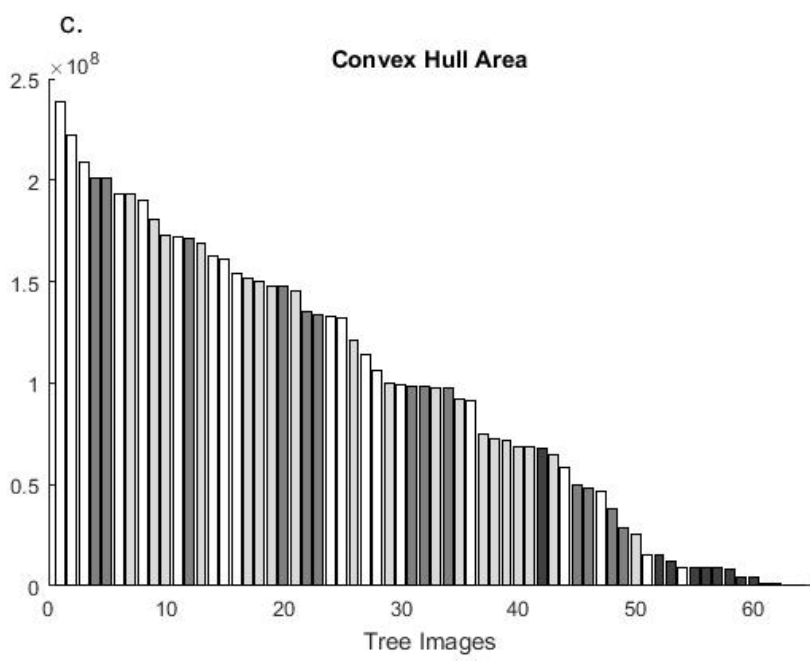
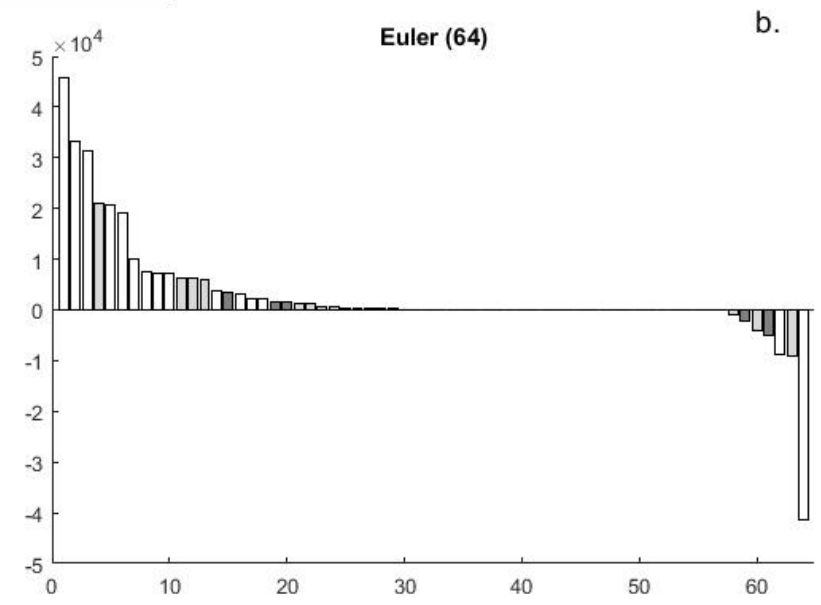
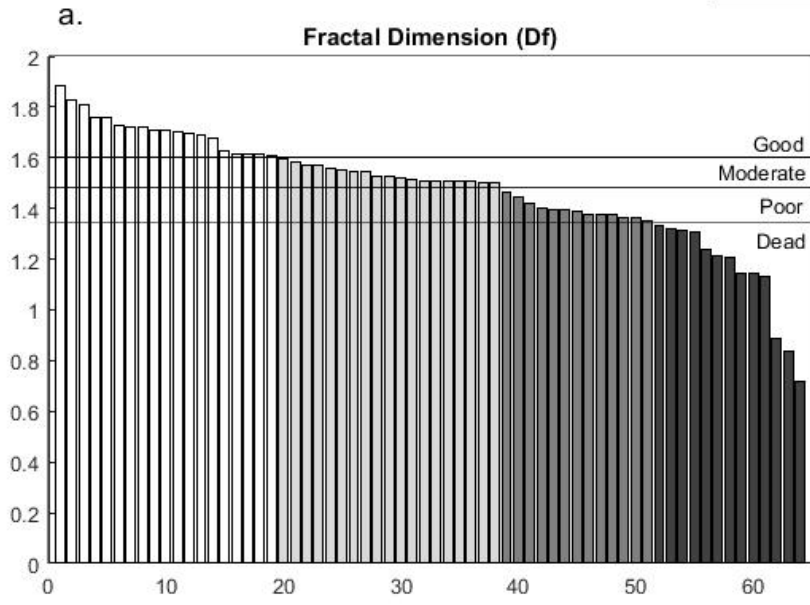
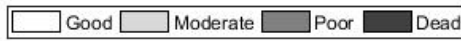
Overall Southern Axis Length – 8 metres

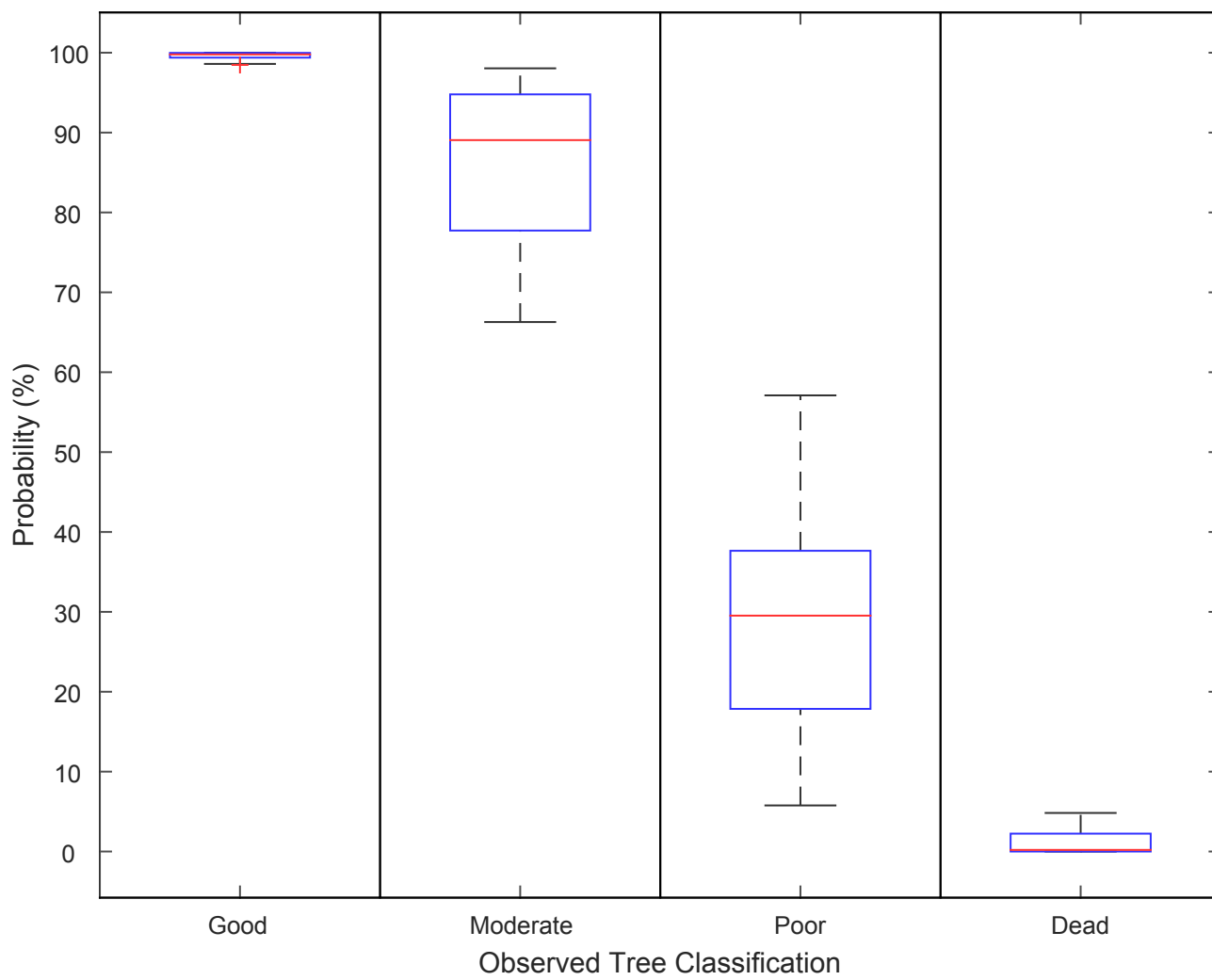


b.









An Objective Methodology for Surveying Trees: Using Fractal Analysis of Crown Images to Measure Structural Condition

Jon Murray^{1*}, George Alan Blackburn¹, James Duncan Whyatt¹ and
Christopher Edwards²

¹ Lancaster Environment Centre, Lancaster University, Lancaster, LA1 4YQ

² School of Computing and Communications, Lancaster University, Lancaster,
LA1 4WA.

*Corresponding author: Tel: +44 1524 652 01; Email: j.murray3@lancaster.ac.uk

Supplementary Information

Image Pre-processing

The pre-processing interventions were applied to the raw images and at each phase of processing were statistically checked for suitability. This procedure focussed on the interventions that were observed to have an effect on the further usability of images in this study. Concurrently, the interventions were also statistically tested for suitability of use in the study.

Quantitative Strength of Pre-processing Phases

In order to establish that the three different pre-processing interventions were having a measurable effect on the data, when applying each pre-processing phase, confidence intervals were calculated using the following formula where n is the sample size and s is the standard deviation:

$$\bar{X} \pm Z \frac{s}{\sqrt{n}} \quad (1)$$

At Figure 1, the pre-processing interventions are represented as one; for the baseline or uncorrected image Df values; two, after applying a chromatic aberration correction; three, after lens distortion correction; and four, after image sharpening. As shown in Figure 1, there is a general positive effect caused by each of the post processing interventions on the image

Df values. The dataset confidence level at CI95%, suggests that each post processing intervention has a reliable and repeatable influence on the Df values at each successional stage.

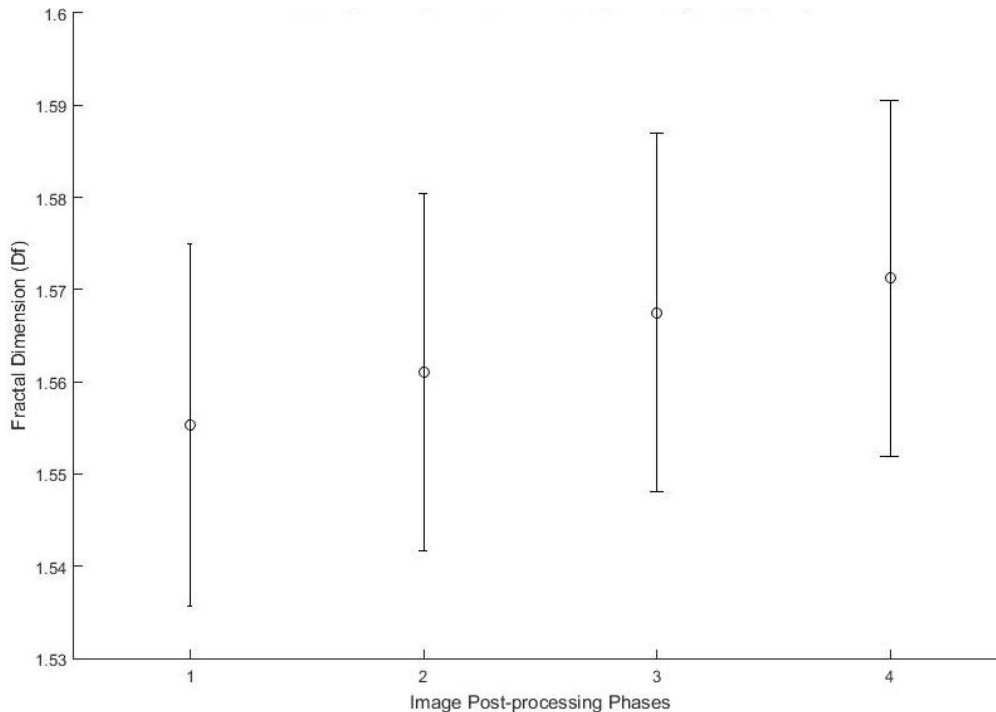


Figure 1 Model testing of the impact of image post processing phases on average Df values, demonstrating 95% confidence interval (CI95%) ($n=247$). Note: Image pre-processing phases applied 1 = raw unprocessed images, 2 = applying chromatic aberration correction, 3 = applying lens distortion correction, 4 = applying image sharpening. The Df values are a logarithmic scale, demonstrated on a truncated axis.

Although the CI bars overlap, potentially suggesting there is no statistical conclusion to be drawn; it should be noted that CI are not a test of statistical significance. A paired, two sample t-test was used assessing the significance between the uncorrected Df data (phase one), and the Df data following the final post processing stage (phase four). The result is a p -value of $p0.005$, therefore that the differences in the effects of the post processing interventions on the Df values are considered very highly significant.

Validity Testing of Pre-processing

In order to quantify the effect of the before and after the phases of post processing, the corrected effect size was calculated using Hedge's g . This test quantifies the effectiveness of the post processing interventions. Hedge's g , follows as:

$$\left(d_s = \frac{\bar{X}_1 - \bar{X}_2}{\sqrt{\frac{(n_1 - 1)SD_1^2 + (n_2 - 1)SD_2^2}{n_1 + n_2 - 2}}} \right) \times \left(1 - \frac{3}{4(n_1 + n_2) - 9} \right) \quad (2)$$

Where SD is standard deviation and n is frequency of values for the two variables; Df values before and after the pre-processing interventions. As can be seen in Figure 2, this results in a large impact on the Df values with the Hedge's g effect size at 2.4504.

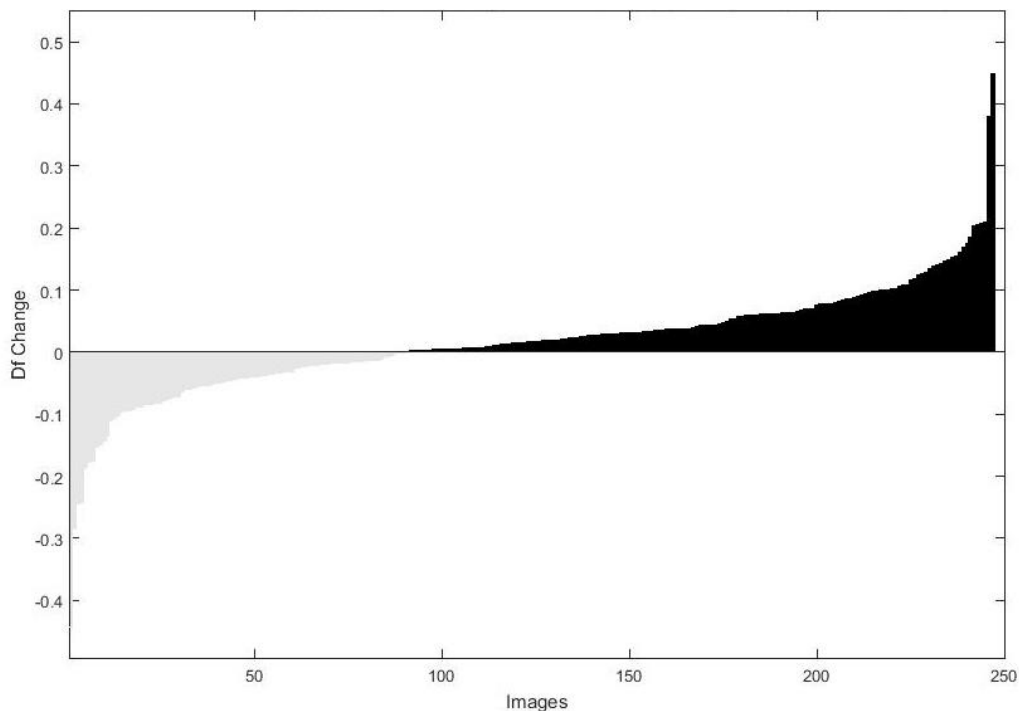


Figure 2 The quantification of effect size following image post processing ($n=247$). The value of Hedge's g at 2.4504 with a confidence interval at 95%, suggests that the pre-processing phases have a significant effect on Df values.

Due to the combination of the assessment of the effect size (Hedge's g 2.4504), supported with a confidence interval of CI95% and a statistical significance of $p < 0.005$, the image post processing phases have had a significant effect on the quality and usability of the images, thereby enabling the images to be used in subsequent analysis within this study.

Model Fitting

Following the pre-processing interventions, the corrected images were reanalysed through generating a second Df score. These are compared with the original, raw Df to identify the extent of residuals between the two data sets in order to estimate the extent of potential statistical error. This phase of the investigation also indicates whether unwanted data noise

has been added in to the Df values, and identifies the correlation of remapping the pre-processed Df back to the raw Df values. As can be observed from Figure 3 the sampled standard deviation of the modelled Df very closely agrees with the original, unprocessed Df values at 0.07% utilising normalised root mean squared error (NRMSE).

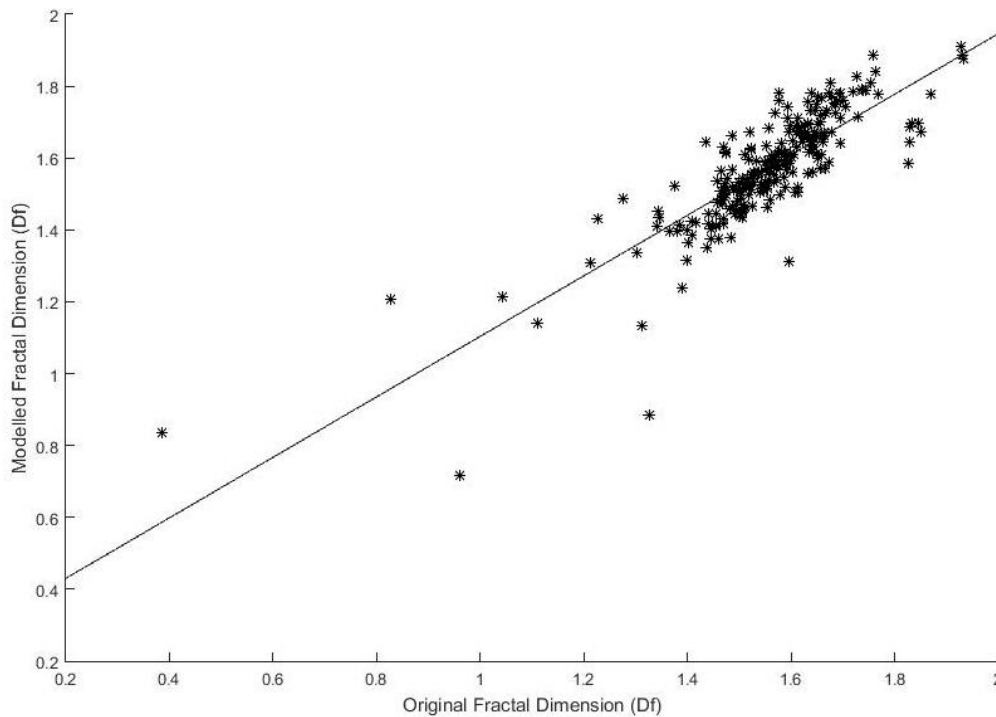


Figure 3 Regression analysis of fractal dimension values following image pre-processing ($n=247$). The pre-processed Df, remains a statically relevant representation of the raw Df values with a normalised root mean squared error (NRMSE) of 0.07% ($y = 0.84*x + 0.26$, $R^2_{adjusted} = 0.7\%$).

Recommended Field and Data Processing Workflow

The development of the techniques used during this research provides an operational methodology for the objective classification of tree structure. This procedure has two phases split between field and office based work (Figure 4). In phase one, using predefined rules for the selection of trees in accordance with the survey requirements, a tree would be selected, photographed at the mid-point of the crown and the image checked in the field using the same field methodology as described earlier in this paper. This process would be repeated for several iterations in order to create a reference data set for each tree species within the survey. The second phase also follows the earlier described process of uploading the tree images (to a desktop computer with the required code), defining a bounding box for the crown area to be analysed and the Df value to be calculated. Finally, to achieve objective classification for the individual trees, the Df values of each tree image would be cross-

checked against the reference data threshold levels of the individual tree species (e.g. Table 2 of main article).

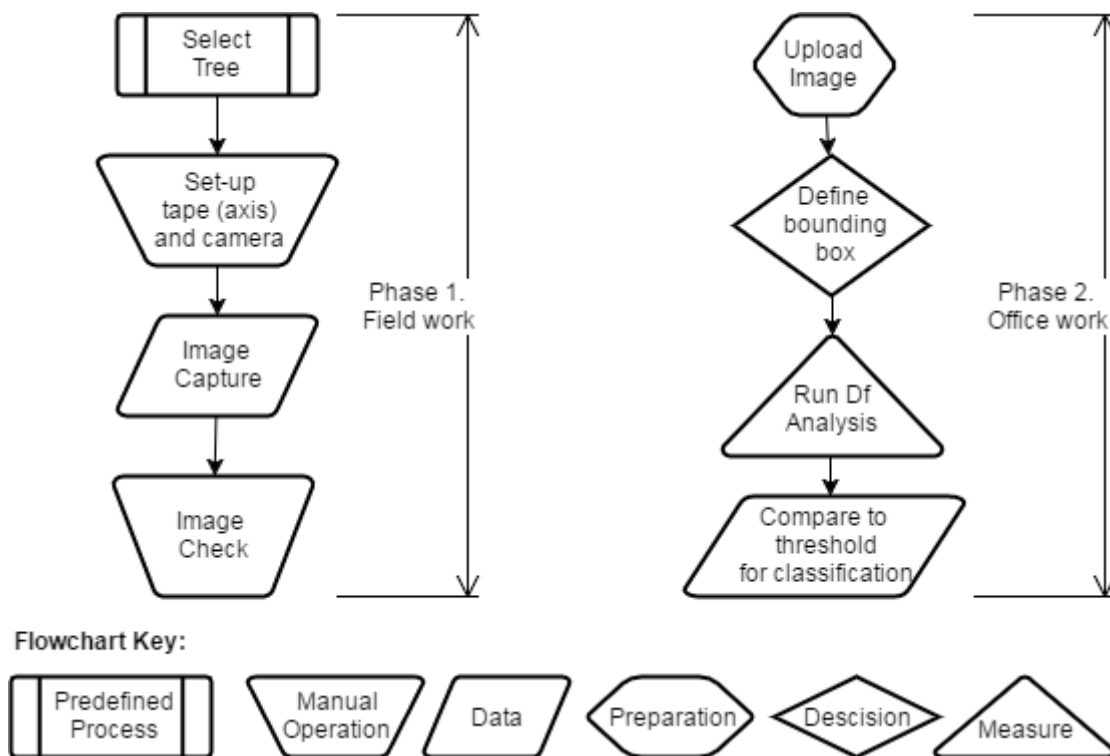


Figure 4 An operational workflow for the field practitioners use of a methodology for the classification of tree crown structure in fractal dimensions (Df), using hemi-spherical photography.